Combined MRI and Optical Computed Tomography: Literature Review

Ciara McErlean

23/1/13

1 Introduction

2 Theory

The theory behind CT reconstruction broadly the same between x-ray CT and OptCT. One minor difference is that it is common in x-ray CT for the detectors to rotate around the sample whereas in OptCT the sample rotates and the detectors are stationary. This introduces a minus sign at one stage of the reconstruction algorithm.

2.1 Radon Space

When light passes through a substance, it is assumed to be attenuated by some small amount of intensity ΔI over a small distance Δy

$$\frac{\Delta I}{I} = \mu(y)\Delta y \tag{1}$$

where $\mu(y)$ is the linear attenuation coefficient. Taking the infinitesimal limit and integrating,

$$\int_{I_0}^{I} \frac{1}{I}\,\mathrm{d}I = -\int_{L} \mu(y)\,\mathrm{d}y \tag{2}$$

this leads to Beers Law

$$I(y) = I_o(y)\mathrm{e}^{-\int_L \mu(y)\,\mathrm{d}y} \tag{3}$$

where I_0 is the intensity with no attenuation and $I(y)$ is the intensity at depth y. L is the path the light ray has followed, the integral in the exponential term of Beer's Law takes into account the differences in attenuation coefficient along the path L.

From equation 3 it is apparent that the intensity of a light beam after passing through a sample gives information about the line integral of the function μ along the line L. The CT scanning process records this information for many lines L at different lateral positions and it is from this information that we reconstruct a map of μ. [6] The Radon transform maps a function into a set of its line integrals. Therefore, CT reconstruction involves an inverse Radon transform.

In order to build up a map of attenuation coefficients, line integrals must be measured from multiple angles (see Figure 1). If the sample rotates by some angle ϕ then the attenuation seen at position (x, y) changes.

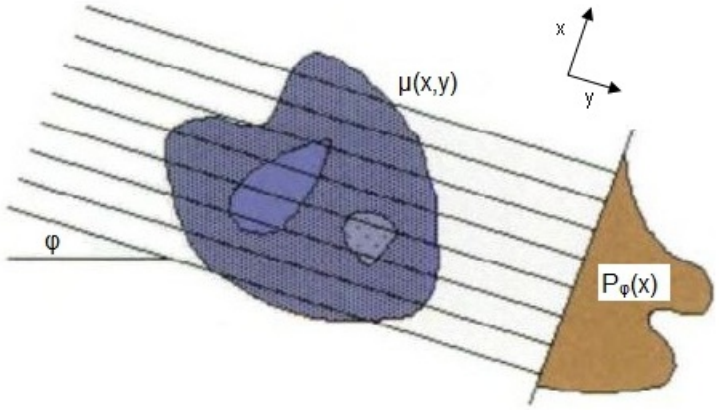

Figure 1: Parallel ray geometry showing how a projection/view, $P_\phi(x)$, is taken at angle ϕ. The attenuation $\mu(x, y)$ within the sample is not uniform and projections must be taken from many angles to reconstruct a map of $\mu(x, y)$. Here x represents lateral position and y represents depth. Figure adapted from [15].

The Radon transform, often called a projection or a view, is defined as

$$P_\phi(x) = \int\limits_{sample} \mu(x', y')\,\mathrm{d}y = -\ln\left(\frac{I_\phi(x)}{I_0}\right) \tag{4}$$

where

$$\begin{aligned} x' &= x\cos\phi + y\sin\phi \\ y' &= -x\sin\phi + y\cos\phi \end{aligned} \tag{5}$$

The projection information is stored in what is known as 'Radon space' with dimensions (x, ϕ). Radon space is filled by measuring the projection value for all combinations of x and ϕ. A filled Radon space diagram is often referred to as a sinogram (see Figure 2).

In practice, the finite number of lines L limits the resolution of reconstructions. There are two geometries for 2-D reconstructions; parallel beam and fan beam. The choice of scanning geometry also affects the resolution. [6]

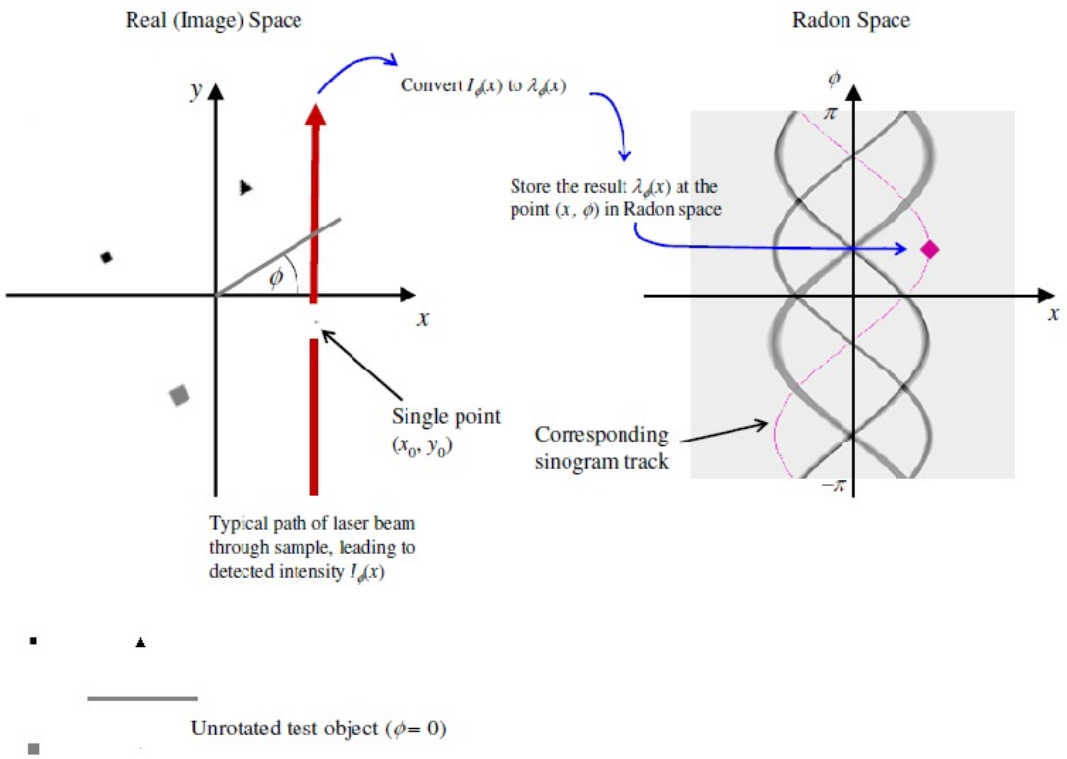

Figure 2: Transformation from image space to Radon space demonstrated. Projection information is stored in Radon space. A 2-D image of Radon space is often called a sinogram. Different shapes produce characteristic tracks on the sinogram according to how they look when rotated. Figure adapted from [26]

2.2 Filtered Back-projection

The information stored in a sinogram is used to reconstruct a map of attenuation within the sample. This is done through the process of back-projection.

Simple back-projection involves simply taking each projection point $P_\phi(x)$ and working back along the line integral which created that projection in real space, attributing each depth with the value $P_\phi(x)$. Doing this for all projection points certain areas in real space are shaded darker as projections from different angles cross over. This builds up a picture of the shapes inside the sample. However, this form of back-projection is flawed, producing blurred images. In order to reconstruct more

accurate images a mathematical trick called Filtered Back-projection (FBP) is used.

FBP

In fact, two assumptions are made to enable the conventional OPT to use the term of projection and the reconstruction algorithm. First, the narrow cones of the light ray projected onto a CCD are assumed to be the strip integrals through the sample. Second, the axes of the light cones are taken to be parallel to each other. The two assumptions place severe constraints on the resolution of OPT imaging. In this paper, we present improved image-forming optics for OPT, with which the axes of the light cones are parallel to the optical axis of the optics. As a result, the parallel integral throughout a sample can be satisfied, and the second assumption mentioned above is relaxed. This method results in an improved spatial resolution, especially for the cross sections far from the optical axis. [7]

Walls 2005 [8] : *the tOPT views must be transformed according to Beers law, standard in x-ray CT, in order to obtain sums of attenuation coefficients along the projection cones, necessitating sample removal and capture of brightfield images. Each view is divided by a low noise estimate of the illumination that is obtained by averaging several brightfield images.*

Fourier slice theorem requirements, see Wang 2007 [9]

Nyquist sampling theory dictates minimum number of projection/views required.

Computational methods for improving reconstructions in OPT by Birk in 2011 [10]

2.3 Refractive index matching

2.4 Optics

(See Walls 2007) Resolution given by Rayleigh criterion.

$$r_{Airy} = \frac{0.61 n \lambda}{NA} \tag{6}$$

where r_{Airy} is the radius of the Airy function which is a measure of resolution in the focal plane. n is the refractive index of the medium around the lens, λ is the wavelength of light and NA is the numerical aperture of the lens.

Depth of field (DOF) is given by [REF]

$$DOF = n_{bath}(\frac{n\lambda}{NA^2} + \frac{n}{MNA}e) \tag{7}$$

where e is the pixel size of the CCD, n_{bath} is the refractive index of the medium surrounding the specimen and M is the lateral magnification.

According to Nyquist the Airy disc must be sampled more than twice per DOF distance to avoid aliasing. This constrains the detector spacing to

$$e \leq M\frac{r_{Airy}}{2} \tag{8}$$

so the maximum possible DOF is given by

$$DOF_{max} = n_{bath}(\frac{1.305\lambda}{NA^2}) \tag{9}$$

Shows trade-off between high resolution with high NA and high DOF with low NA. Generally choose NA based on size of sample.

2.5 Common artefacts

Axis of rotation problems. Corrections suggested by many groups. Recently by Dong in 2012 [11] discuss method.

Walls 2005 *Noise is Poisson distributed below 2% on an averaged signal. Therefore artefactual effects must be kept below 1%*

3 Dosimetry

3.1 Laser scanning configuration

One of the first reported optical computed tomography (OptCT) systems was developed in the area of gel dosimetry. Accurate 3-D measurement of dose delivery in radiotherapy is extremely important in developing safe treatment plans. Specialist polymer gels, such as BANG® [12], respond to irradiation with changes in optical attenuation and scattering properties. This makes them ideal for measuring 3-D dose distributions. Previously the irradiated gels were measured by MRI and x-ray CT however, these are expensive imaging modalities. In 1996, Gore and Maryanski published the first system for scanning polymer gels using optical computed tomography. [13] In later comparisons, OptCT has been found to be more precise, have reduced noise and smoother line profiles than MRI for gel dosimetry. [14]

Gore's system consisted of a He-Ne laser source and large area photodiode detector (see Figure 3). Translate-rotate acquisition was employed whereby the sample was rotated and projection data acquired by the photodiode over 360°. The smaller the angular steps between projections, the more accurate the reconstruction. [15] For a 2-D reconstruction, projections are acquired for multiple spots across a slice of the sample by translating the laser beam using mirrors. For 3-D information, the sample height had to be manually adjusted and many 2-D slices acquired. This meant scanning an entire sample took hours and lengthy scanning times are the chief disadvantage of the laser scanning method. Accuracy of 5% is reported and spatial resolution of 2mm, which is roughly the same as the laser beam width. [13]

The idea of OptCT scanning in dosimetry was quickly developed by other groups. Laser scanning set-ups were published in 1996 by Tarte *et al.*, [16] and Kelly *et al.* [REF] *Can't find the paper 1996 Kelly references in 1998 [17] Med Phys says it doesn't exist.* Kelly *et al.* claim to have independently developed their scanner which is very similar to that of Gore's. In in both Kelly's and Tarte's scanners, the sample is rotated and translated using a stage whereas Gore used mirrors to translate the laser spot across the sample.

A commercial laser scanning OptCT system, OCTOPUS™by MGS Research, Inc. (Madison, CT), is an extension of Gore's original set-up with the addition of a platform capable of vertical movement for automated slice-selection. [18] For a number of years it was the only commercially available system and has been characterised

by several groups. [18–21] According to Oldham, characterisation of OptCT systems should include checks on geometric distortion, accuracy of reconstruction, scatter artefacts and reflection and refraction artefacts. [22]

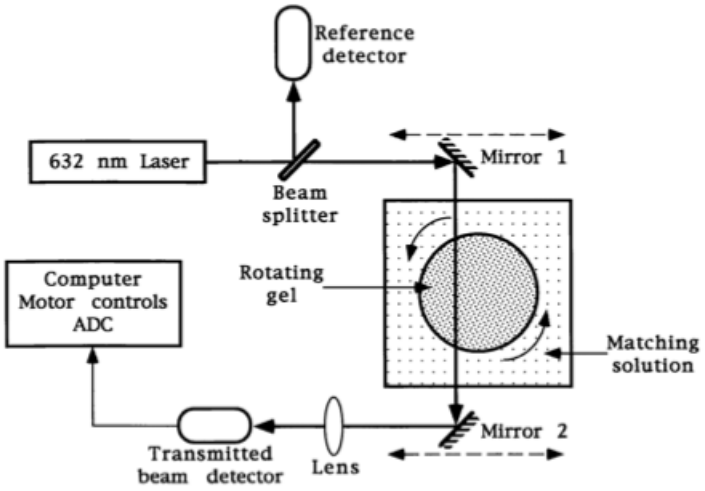

Figure 3: A first generation, Laser Scanning OptCT system developed by Gore. The sample is rotated and projections recorded at a number of angles. The mirrors scan the laser beam across the sample but movement in the vertical direction is by manual adjustment only (figure from [13]).

Laser scanning systems include a beam splitter before the sample to create a reference beam. Dividing projections by the reference intensity corrects for laser beam intensity fluctuations. [13]

Refraction and reflection at container walls are significant concerns for all configurations of dosimetry with OptCT. Generally, laser beams are incident on the gel container at a small angle, such as 5°, to avoid large reflection at the interface. In addition, the gel container is usually placed in a tank containing 'matching fluid' with a refractive index close to that of the gel. This prevents significant refraction as the light passes into the gel. Doran found through ray tracing simulations that the refractive index of the walls of the matching tank and gel container are not important compared to the gel and matching fluid. The optimum difference in refractive index between these two was calculated to be 0.0025 and not zero as originally thought. [23]

To maximise the dynamic range of the system, food dye is commonly added to the

matching fluid so both the refractive index and optical density of the matching fluid and gel are very similar. [24]

3.2 Pixelated detector based systems

In 1997 the first charge coupled device (CCD) camera based OptCT system was published by Tarte *et al.* which employed an incoherent white light source and CCD camera detection. [25] The advantage of a pixelated detector based system is that an entire 2-D projection can be imaged at once, potentially increasing the scanning speed by several orders of magnitude depending on the data through-put rate. Tarte's system used a divergent light source and diffusing screen to measure optical density in a thin gel section (see Figure 4).

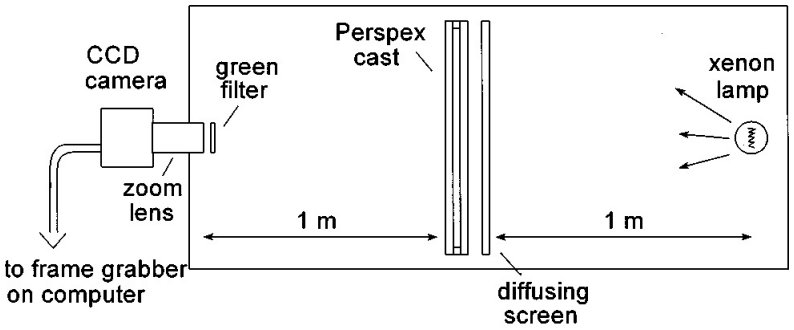

Figure 4: Diagram of the first CCD-based OptCT system, developed by Tarte *et al.* It uses divergent illumination from a white light source and CCD camera detection to record an entire 2D projection at once (figure from [25]).

The accuracy of Tarte's system was checked by comparison with the standard measure of dosimetry, the parallel plate ionisation chamber. It was found to be on average within 3% of the value from the ionisation chamber. [25] A comparison between Tarte's laser scanning and CCD set-ups found that they had similar spatial resolutions. The CCD method had improved speed of acquistion but suffered from consistently worse SNR as a photodiode detector can collect many more photons per 'pixel' than a CCD camera. [25]

Advances in technology have meant that high quality detectors are much more affordable. A cheaper alternative to very high quality CCD cameras is the CMOS

(Complementary Metal-Oxide-Semiconductor) detector which has the potential for higher resolution and dynamic range. [26] Using a higher quality detector would improve many OptCT systems in terms of scanning speed and reduced artefacts. [23,25]

Parallel beam configuration: One method to reconstruct 3-D images with a CCD or CMOS detector is to create a broad parallel beam. This allows the use of parallel reconstruction algorithms, very similar to those used for x-ray CT. Each 2-D projection image recorded corresponds to one row for every slice in the 3-D reconstruction sinogram. [26] Telecentric optics, in which the chief rays are parallel to the optical axis, are key in the design of this configuration. [8] Telecentric optics can be achieved either through a careful arrangement of a large converging lens before the sample and standard camera lens [23] (see Figure 5) or through an expensive telecentric lens [27]. The process of forming a parallel beam results in non-uniformities in the lightfield. This is compensated for by subtracting a 'correction' or 'open lightfield', image which is a projection taken with no sample in the tank. [23]

Telecentric lenses have two advantages for the purpose of parallel ray computed tomograhy: they provide a near constant perspective across the field of view, and the image magnification is constant with sample depth. [4]

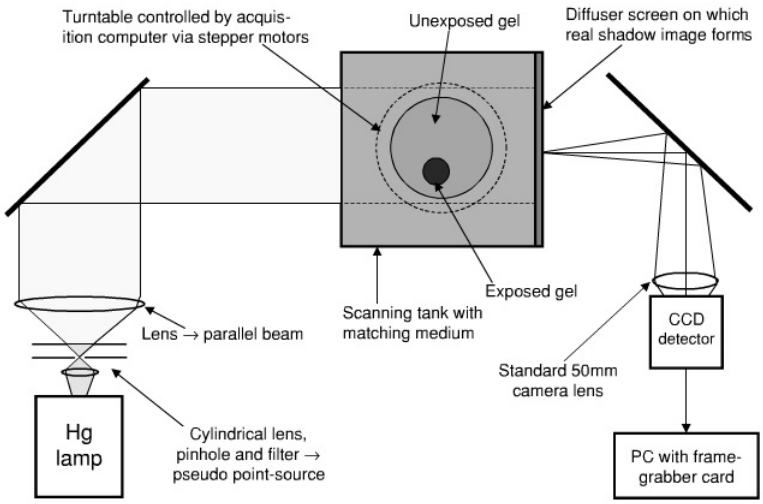

Figure 5: Diagram of a parallel beam OptCT system, developed by Doran *et al.* Telecentric optics create a parallel beam (figure from [23]).

Initial systems suffered from 'graininess' due to the unstable gain of cheap CCD cameras and granularity of the diffusing screen. [23] Doran *et al.* proposed some methods of correcting these problems. Oscillating the diffuser screen at high frequency "'smears' out the granularity" while randomly horizontally displacing the CCD camera by a few pixels between acquisitions can reduce the effect of 'bad' pixels. [23] The parallel configuration appears to be more susceptible to schlieren artefacts caused by refractive index inhomogeneities in the sample. [28]

Cone beam configuration: Wolodzko *et al.* published the first cone beam OptCT system with CCD detection for gel dosimetry. [29] One advantage of this configuration is the optics for producing a cone beam are much simpler than those for producing accurate parallel beams. [26] However, the reconstruction is computationally more complex. [30] A commercial cone-beam system, Vista^{TM}by Modus Medical Devices Inc. (London, ON, Canada), is available and reviewed recently by Olding *et al.* [31]

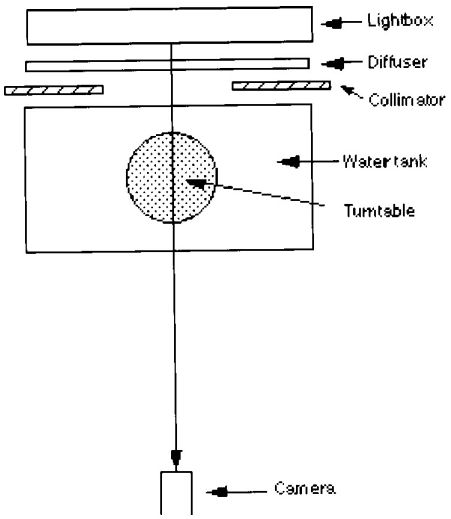

Figure 6: Cone-beam CCD configuration (figure from [29]).

When pixelated detectors are used, there appears to be more literature based on the parallel beam configuration than cone-beam. Although there has not been experimental comparison of the two Doran suggests that while cone-beam is usually somewhat cheaper due to simplified optics, modern parallel-beam systems have better scatter-rejection and may have fewer stray light problems. [26, 31, 32]

4 Tissue imaging

4.1 Optical Projection Tomography

Another version of OptCT was developed by Sharpe *et al.* in the area of 3-D microscopy for gene expression studies. [33] Although this set-up in 2002 came after Gore's they are apparently independent and Sharpe named his technique Optical Projection Tomography (OPT).

Other techniques for 3-D microscopy are well established however, OPT offers some unique advantages. Confocal microscopy is offers high resolution images up to a depth of about 1mm. [34] However, it is limited to fluorescent signals meaning many optical stains used routinely in histology would not work. Optical coherence tomography (OCT), which is commonly used in ophthalmology, is capable of micrometer-scale resolution with depth limited to 2-3mm in tissue. [35] Both of these techniques generate tomographic images through sectioning whereas OPT is a projection based tomography technique. [36] Avoiding sectioning is important in producing truly representative 3-D images. [4] Another advantage of OPT is its ability to image much larger specimen, with depth of around 3cm being reported. [4]

Sharpe's original system uses a microscope to focus projections of a mouse embryo onto a camera imaging chip (CIC). Image-focusing optics are one difference between OPT and x-ray CT, which records shadows of the sample. [33] Sharpe reports some impressive images seen in Figure 7. Use of the microscope gives resolution of about 5-10μm meaning single-cell membranes, around 10μm thick, can be seen. [33] However, the high NA optics which give high resolution limit the depth of field (DOF). Sharpe decided to circumvent the problem of a low DOF by positioning the rotational axis so only half the specimen was in focus at once and the specimen was scanned 360° to collect in-focus data from all points. The problem with only having half of specimen in focus at once is that unfocused light is superimposed upon the focused data and included in the reconstruction. This leads to blurring which is worse with distance from the axis of rotation. Walls proposed a method of correcting this defocusing effect using a frequency-distance filter, as described by Xia for SPECT. [37, 38] The filter narrows the PSF to in-focus data allowing in-focus, high resolution images to be reconstructed. [38]

In dosimetry the refractive index within the polymer gels was roughly uniform. In tissue this is not the case, with scattering and refraction occurring at cell membrane

interfaces. To make high resolution reconstruction through back projection possible, light paths through the specimen must be able to be approximated as parallel line integrals, meaning refraction must be minimised. A process called optical clearing or clarification is employed which renders tissue optically transparent. An optical clearing agent (OCA) replaces the lower refractive index intra-cellular fluid acting as a matching fluid within the sample itself. The mechanism for this differs between agents, see Section 5 for more detail.

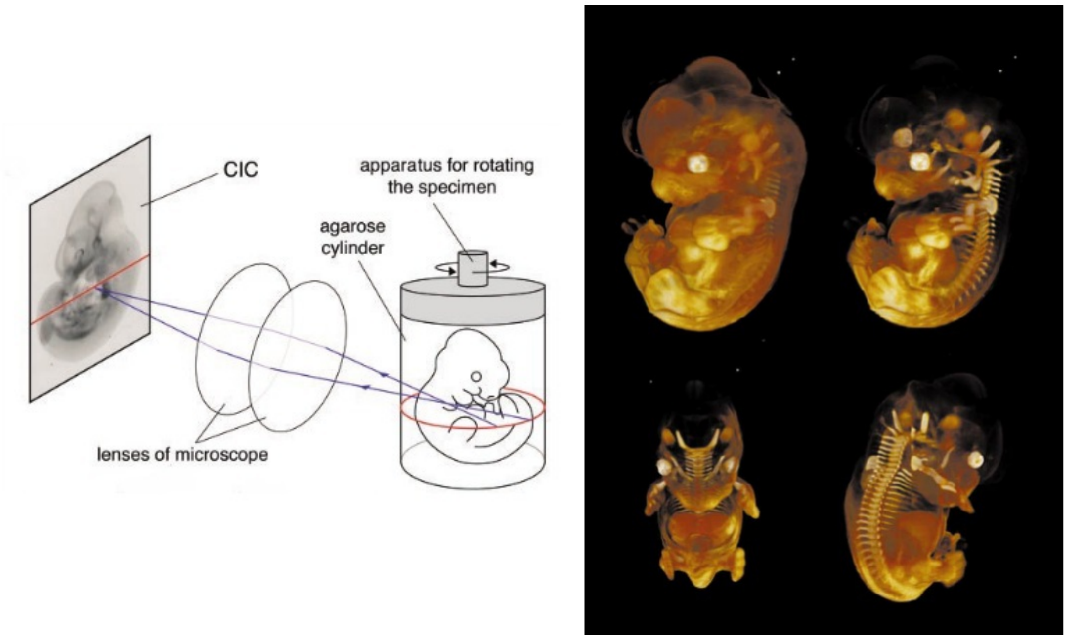

(a) OPT setup (b) Mouse images

Figure 7: Part (a) shows the optical set-up for the first OPT system by Sharpe. CIC indicates the camera imaging chip. A microscope is used to focus projection images onto the CIC. The specimen is set in agarose gel for stability. Figure adapted from [33]. Part (b) shows some false colour images of a TS21 mouse embryo stained with alcian blue and imaged with OPT. The images have varying degrees of opacity allowing control of which internal organs are seen. Figure adapted from [36].

In 2005 Fauver reported a modified version of OPT capable of imaging single cell nuclei with 0.9μm resolution (see Figure 8). [39] The OPT microscope includes a rotation stage and piezoelectrically driven objective lens. In a technique similar to Hausler [40] the objective lens is scanned axially to create an extended DOF image

which is also known as a pseudoprojection. The extended DOF means features have the same focus from all angles, allowing high resolution reconstruction. However, this is not a truly quantitative technique, hence pseudo and not true projections are recorded. A high numerical aperture (NA) lens gives high resolution at the expense of low depth of field. If such high resolution is not required, low NA optics such as those used by Sharpe would be a more quantitative way to generate projections than scanning a high NA lens.

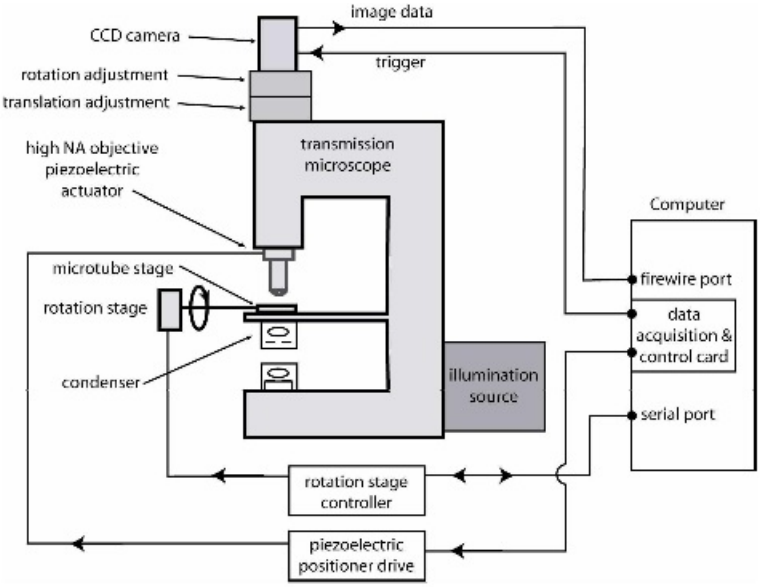

Figure 8: OPT microscope for imaging single cell nuclei. A microcapillary tube injected with cells is rotated with sub-micron precision and refractive index matching to 0.02. The piezoelectric objective lens is scanned axially to create extended depth of field images (figure from [39]).

Wang and Wang report an improvement to OPT giving higher axial and lateral resolution, even for slices far from the optical axis. [7,9] As previously mentioned, to obtain high quality reconstructions the projections should closely approximate a line integral of parallel rays passing through the sample. [7] This is not exactly the case for OPT, limiting the best resolution possible. Wang proposed placing an iris at the back focus of the objective lens. This reduces divergence of the projection rays from paths parallel to the optical axis giving qualitatively better resolution.

4.2 Fluorescent/emission OptCT

Sharpe was the first to identify the possibility of using OPT to image fluorescent stains in biological specimen. [33] There are a wide range of fluorescent optical stains in use in histology making this development particularly useful for biological imaging. It also offers the advantage of being able to record multiple signals independently unlike transmission OPT (tOPT). [33]

Optical emission CT (OptECT) also known as emission OPT (eOPT) is the optical equivalent of SPECT (single photon emission computed tomography). [4] Instead of measuring the attenuation of photons through a sample (tOPT), eOPT signal comprises of fluorescence photons emitted along a ray path. [8]

Some changes from the set-up (see Figure 9) from tOPT include the addition of a narrow bandwidth excitation filter before the sample. This selects for the excitation wavelength of the fluorescent marker being used in the sample. The illumination is perpendicular to the detector to avoid detection of the illumination light rather than fluorescence. An emission filter before detector selects for the longer emission wavelength of the fluorophores, again to avoid contamination from auto-fluorescent and ambient photons being picked up by the CCD. To avoid photobleaching systems often include a shutter to turn off the lamp when not imaging. The image forming optics is the same as for tOPT, although the reconstruction and artefacts are different. [8]

Oldham *et al.* have made several improvements on Sharpe's eOPT set-up by changing from microscope to bench-top apparatus. [4, 5] Microscope based systems suffer from poor DOF as the optics are designed to image flat samples. Oldham's custom made set-up, which is closer to the dosimetry systems previously seen, employs telecentric optics giving much improved DOF capable of imaging samples up to 3cm. [4] However, better DOF is achieved at the cost of worse lateral spatial resolution and this trade-off must be considered with respect to the information required from the specimen. [24]

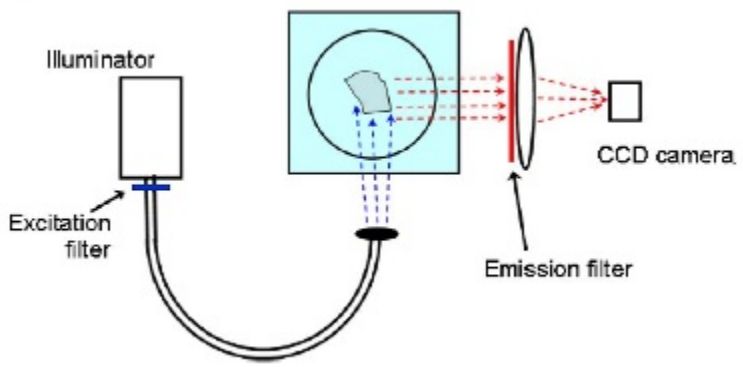

Figure 9: Example of setup for OptECT/eOPT imaging. Filters are used to select for the excitation and emission wavelengths of the fluorescent stain. This set-up can give an image but no quantitative information without specialised reconstruction techniques discussed below. Figure adapted from [4].

There are several reasons why eOPT data is not quantitative. The most significant problem is that an unknown number of emitted photons are attenuated within the sample. This requires a mathematical model of attenuation for correction. The second problem is that some incident photons are attenuated before they can cause excitation. This can be compensated for with simultaneous illumination from multiple angles. [41] Another problem identified by Darrell *et al.* is a defocusing effect caused by the lower intensity of of fluorophores positioned outside of the focal plane. Darrell's method of quantifying eOPT data invloved a Fourier optics based model which accounted for the defocusing effect and isotropic emission attenuation. [42] A weighting function was calculated based on this model. The function was used in FBP and acts as a window function, spreading the projection information unevenly over the reconstruction image plane.

Kim *et al.* have also published a method for correction of emission attenuation. [41] This method is similar to those used for attenuation correction in SPECT. A co-registered image from tOPT is used to construct an attenuation map and calculate attenuation-survival probabilities for the sample. The probabilities are then used in an iterative OSEM (ordered-subsets expectation-maximisation) reconstruction. [41, 43] This attenuation correction method was tested using a phantom with known fluorescent fibres and corrected images showed more uniform intensity across the three fibres, differing by 4% in the corrected images but as much as 24% in uncorrected data. [41]

In an extension of Kim's method, Thomas *et al.* were the first to report a comprehensive correction for eOPT. [44] Their iterative method corrects for both emission and excitation attenuation and non-uniformities in the light source. Tests of their technique using phantoms show that it can give quantitative information of 3-D fluorophore concentration. This is could be very biologically useful, for example looking at uptake of drugs in tumour treatment. **[REF]**

There have been attempts at performing OPT on live specimen. [45–47] The chief difficulties in this are developing a method limiting scatter and refraction whilst also keeping the specimen alive. Boot and Sharpe reported their efforts for *in vitro* time-lapse quantitative eOPT imaging through tracking GFP expression of a growing mouse embryo limb bud, about 1mm in size. [45] Live OPT has also been used in molecular imaging tracking a changing 3-D gene expression pattern. [47] Vinegoni *et al.* reported *in vivo* imaging of Drosophila melanogaster pupae without clearing or matching fluids. [46] As there is no clearing involved and a mathematical model is required for reconstruction Vinegoni called this 'mesoscopic' imaging rather than OPT/OptCT. Although gathering some biologically interesting information, the resolution was much worse than conventional OPT limiting the applications for this technique.

5 Optical Clearing

Optical clearing or clarification is a very important step in OptCT imaging of tissue. Tissue are made up of many components of different refractive indices meaning there are many optical boundaries for scatter and refraction to occur at. This is the reason why visible wavelength light does not penetrate very far in tissue. In order for the parallel ray assumption used in CT reconstruction to be true, refraction and scatter at cell membrane interfaces within the sample must be minimised. [5] This is accomplished with clearing.

During clearing, intracellular fluid is replaced with a optical clearing agent (OCA). There are many choices of OCA but they should all have refractive indices matching the tissue to be imaged and be hyperosmolar (i.e. have a very high solute concentration).

A very popular technique for clearing is the Optical Immersion technique. The sample is set in agarose gel for stability. The gel contains pores which allows diffusion of the OCA. The most commonly used OCAs for OPT are benzyl-alcohol-benzyl-benzoate (BABB, refractive index 1.55) or methyl salicylate (MetSal, refractive index 1.53). These are both aromatic organic solvents and are not miscible in water. Therefore a graded sequence of ethanol and OCA solutions is required to replace the intracellular water with the OCA. [5]

Some OCAs including glycerol and DMSO (dimethyl sulfoxide) can be directly applied to the tissue without need for graded ethanol solutions. However, they have been shown to be less effective than BABBs and MetSal and cannot penetrate deeper than 1cm. [5] [MORE REFS?] They may be more suitable for *in vivo* or live studies.

BABB has n=1.56 while water is n=1.33, what is n for tissue? [8]

Clearing for OptECT: [48] [49]

6 Optical Staining

Sharpe 2002 stains for gene expression and limb bud growth.

Discuss which stains are relevant for cancer biomarkers. [50]

Being able to use optical stains is extremely useful for computer recognition of organs, can pick better thresholds. [36]

Soufan 2003 [51] gene expression during cardiac development. Highlights problem of whole-mount staining not working for all stains. Depends on size of specimen. Therefore, they took slices of embryo heart.

Oldham 2007ku: *Optical labeling of organ microvasculature was achieved using two stains deposited via natural in vivo circulatory processes: a passive absorbing ink-based stain and an active fluorescin FITC-lectin conjugate. The lectin protein binds to the endothelial lining, and FITC fluorescense enables optical-ECT imaging. first staining step was achieved by administering a contrast or labeling agent to the live animal e.g. by tail vein or carotid artery cannulation such that the stain is deposited by natural circulation of the blood..... Two stains have been evaluated: a passive light-absorbing stain based on an isotonic ink solution and an active FITC-lectin conjugate, where the lectin actively binds to endothelial cells and the FITC protein can be stimulated to emit fluorescent light. The agents were allowed to circulate for about 4 to 5 min prior to sacrificing the animal. The tissue of interest was then removed for the second preparation step of optical clearing.*

Sharpe demonstrated the possiblilty of using fluorescent markers in combination with a fluorescent microscope to image *E10.5 embryo stained for HNF3 and neurofilament proteins. Filter sets were chosen to selectively image the two fluorochromes used (Alexa 488 and Cy3), and a third set was used to record the autofluorescence emitted by all the tissue.*

Kim 2008 *GFP and RFP filters used to see HIF1 and necrotic regions respectively. tumour cell line had been genetically labelled (pre-implantation) with fluorescent reporter genes such that all viable tumour cells expressed constitutive red fluorescent protein and hypoxia-inducible factor 1 transcription-produced green fluorescent protein. In addition to the fluorescent reporter labelling of gene expression, the tumour microvasculature was labelled by a light-absorbing vasculature contrast agent delivered in vivo by tail-vein injection.*

Oldham xenograph 2006 - more details on staining in paper. optically cleared in a key process to make the samples amenable to light transmission. The cleared tumors were imaged in three modes (i) optical-CT to image the 3D distribution of microvasculature as indicated by absorbing dye, (ii) optical-ECT using the FITC excitation and emission filter set, to determine microvasculature as indicated by lectin-endothelial binding, and (iii) optical-ECT using the DSRed2 filter set to determine the 3D distribution of viable tumor as indicated by RFP emission.

7 Recent Research

Imperial group investigating Opt combined with FRET and FLIM. Define these and some uses for the combined modality. What physical/software changes needed for this imaging. FLIM OPT: [52], In vivo FLIM OPT [53].

Time gated OPT Bassi 2010 [54]

CLAHE Hornblad 2011 [55]

Lorbeer - SLOT [56]

8 Conclusions

References

[1] S R Ray and H G Semerjian. Laser tomography for simultaneous concentration and temperature measurement in reacting flows. In *American Institute of Aeronautics and Astronautics, Thermophysics Conference, 18 th, Montreal, Canada*, 1983.

[2] S Kawata, O Nakamura, T Noda, H Ooki, K Ogino, Y Kuroiwa, and S Minami. Laser computed-tomography microscope. *Applied optics*, 29(26):3805–3809, 1990.

[3] C S Brown, D H Burns, F A Spelman, and A C Nelson. Computed tomography from optical projections for three-dimensional reconstruction of thick objects. *Applied optics*, 31(29):6247–6254, 1992.

[4] M Oldham, H Sakhalkar, Y M Wang, P Guo, T Oliver, R Bentley, Z Vujaskovic, and M Dewhirst. Three-dimensional imaging of whole rodent organs using optical computed and emission tomography. *Journal of Biomedical Optics*, 12(1):014009, 2007.

[5] M Oldham, H Sakhalkar, T Oliver, Y M Wang, J Kirkpatrick, Y Cao, C Badea, G A Johnson, and M Dewhirst. Three-dimensional imaging of xenograft tumors using optical computed and emission tomography. *Medical Physics*, 33(9):3193, 2006.

[6] F. Natterer. *The Mathematics of Computerized Tomography*. Classics in Applied Mathematics. Society for Industrial and Applied Mathematics, 2001.

[7] Y Wang and R Wang. Imaging using parallel integrals in optical projection tomography. *Physics in Medicine and Biology*, 51(23):6023–6032, October 2006.

[8] J R Walls, J G Sled, J Sharpe, and R M Henkelman. Correction of artefacts in optical projection tomography. *Physics in Medicine and Biology*, 50(19):4645–4665, September 2005.

[9] Y Wang and R K Wang. Optimization of image-forming optics for transmission optical projection tomography. *Applied optics*, 46(27):6815–6820, 2007.

[10] U Jochen Birk, A Darrell, N Konstantinides, A Sarasa-Renedo, and J Ripoll. Improved reconstructions and generalized filtered back projection for optical projection tomography. *Applied optics*, 50(4):392–398, 2011.

[11] D Dong, S Zhu, C Qin, V Kumar, J V Stein, S Oehler, C Savakis, J Tian, and J Ripoll. Automated Recovery of the Center of Rotation in Optical Projection Tomography in the Presence of Scattering. 2012.

[12] M J Maryanski, Y Z Zastavker, and J C Gore. Radiation dose distributions in three dimensions from tomographic optical density scanning of polymer gels: Ii. optical properties of the bang polymer gel. *Physics in medicine and biology*, 41(12):2705, 1999.

[13] J C Gore, M Ranade, and M J Maryanski. Radiation dose distributions in three dimensions from tomographic optical density scanning of polymer gels: I. Development of an optical scanner - Abstract - Physics in Medicine and Biology - IOPscience. *Physics in medicine ...*, 1999.

[14] M Oldham, J H Siewerdsen, A Shetty, and D A Jaffray. High resolution gel-dosimetry by optical-CT and MR scanning. *Medical Physics*, 28(7):1436, 2001.

[15] J C Russ. *The Image Processing Handbook*. Image Processing Handbook. Crc Press, 2002.

[16] B J Tarte, P A Jardine, and T van Doorn. Laser-scanned agarose gel sections for radiation field mapping. *International Journal of Radiation Oncology* Biology* Physics*, 36(1):175–179, 1996.

[17] R G Kelly, K J Jordan, and J J Battista. Optical CT reconstruction of 3D dose distributions using the ferrous–benzoic–xylenol (FBX) gel dosimeter. *Medical Physics*, 25(9):1741–50, September 1998.

[18] K T S Islam, J F Dempsey, Manisha K Ranade, M J Maryanski, and D A Low. Initial evaluation of commercial optical CT-based 3D gel dosimeter. *Medical Physics*, 30(8):2159, 2003.

[19] Y Xu, C Wuu, and Marek J Maryanski. Determining optimal gel sensitivity in optical CT scanning of gel dosimeters. *Medical Physics*, 30(8):2257, 2003.

[20] Y Xu, C S Wuu, and M J Maryanski. Performance of a commercial optical CT scanner and polymer gel dosimeters for 3-D dose verification. *Medical Physics*, 31(11):3024, 2004.

[21] H S Sakhalkar, J Adamovics, G Ibbott, and M Oldham. A comprehensive evaluation of the PRESAGE/optical-CT 3D dosimetry system. *Medical Physics*, 36(1):71, 2009.

[22] M Oldham. Optical-CT scanning of polymer gels. *Journal of Physics: Conference Series*, 3:122–135, November 2004.

[23] S J Doran, K K Koerkamp, M A Bero, P Jenneson, E J Morton, and W B Gilboy. A CCD-based optical CT scanner for high-resolution 3D imaging of radiation dose distributions: equipment specifications, optical simulations and preliminary results. *Physics in Medicine and Biology*, 46(12):3191–3213, November 2001.

[24] N Krstajić and S J Doran. Focusing optics of a parallel beam CCD optical tomography apparatus for 3D radiation gel dosimetry. *Physics in Medicine and Biology*, 51(8):2055–2075, April 2006.

[25] B J Tarte, P A Jardine, T van Doorn, K N Nitschke, and M G Poulsen. Development of a CCD array imaging system for measurement of dose distributions in doped agarose gels. *Medical Physics*, 24:1521, 1997.

[26] S J Doran. The history and principles of optical computed tomography for scanning 3-D radiation dosimeters: 2008 update. *Journal of Physics: Conference Series*, 164:012020, June 2009.

[27] H S Sakhalkar and M Oldham. Fast, high-resolution 3D dosimetry utilizing a novel optical-CT scanner incorporating tertiary telecentric collimation. *Medical Physics*, 35(1):101, 2008.

[28] N Krstajić and S J Doran. Fast laser scanning optical-CT apparatus for 3D radiation dosimetry. *Physics in Medicine and Biology*, 52(11):N257–N263, May 2007.

[29] J G Wolodzko, C Marsden, and A Appleby. CCD imaging for optical tomography of gel radiation dosimeters. *Medical Physics*, 26:2508, 1999.

[30] J Hsieh. *Computed Tomography: Principles, Design, Artifacts, and Recent Advances*. SPIE Press monograph. SPIE Press, 2003.

[31] T Olding and L J Schreiner. Cone-beam optical computed tomography for gel dosimetry II: imaging protocols. *Physics in Medicine and Biology*, 56(5):1259–1279, February 2011.

[32] A Thomas, J Newton, and M Oldham. A method to correct for stray light in telecentric optical-CT imaging of radiochromic dosimeters. *Physics in Medicine and Biology*, 56(14):4433–4451, June 2011.

[33] J Sharpe. Optical Projection Tomography as a Tool for 3D Microscopy and Gene Expression Studies. *Science*, 296(5567):541–545, April 2002.

[34] R H Webb. Confocal optical microscopy. *Reports on Progress in Physics*, 59:427–471, 1996.

[35] D Huang, E A Swanson, C P Lin, J S Schuman, W G Stinson, W Chang, M R Hee, T Flotte, K Gregory, C A Puliafito, et al. *Optical coherence tomography*. PhD thesis, Massachusetts Institute of Technology, Whitaker College of Health Sciences and Technology, 1993.

[36] J Sharpe. Optical projection tomography as a new tool for studying embryo anatomy. *Journal of Anatomy*, 202(2):175–181, February 2003.

[37] W. Xia, R.M. Lewitt, and P.R. Edholm. Fourier correction for spatially variant collimator blurring in spect. *Medical Imaging, IEEE Transactions on*, 14(1):100–115, 1995.

[38] J R Walls, J G Sled, J Sharpe, and R M Henkelman. Resolution improvement in emission optical projection tomography. *Physics in Medicine and Biology*, 52(10):2775–2790, April 2007.

[39] M Fauver, E J Seibel, J R Rahn, M G Meyer, F W Patten, T Neumann, and A C Nelson. Three-dimensional imaging of single isolated cell nuclei using optical projection tomography. *Opt. Express*, 13(11):4210–4223, 2005.

[40] G Häusler. A method to increase the depth of focus by two step image processing. *Optics Communications*, 6(1):38–42, 1972.

[41] E Kim, J Bowsher, A S Thomas, H Sakhalkar, M Dewhirst, and M Oldham. Improving the quantitative accuracy of optical-emission computed tomography by incorporating an attenuation correction: application to HIF1 imaging. *Physics in Medicine and Biology*, 53(19):5371–5383, September 2008.

[42] A Darrell, H Meyer, K Marias, M Brady, and J Ripoll. Weighted filtered backprojection for quantitative fluorescence optical projection tomography. *Physics in Medicine and Biology*, 53(14):3863–3881, June 2008.

[43] H.M. Hudson and R.S. Larkin. Accelerated image reconstruction using ordered subsets of projection data. *Medical Imaging, IEEE Transactions on*, 13(4):601–609, 1994.

[44] A Thomas, J Bowsher, J Roper, T Oliver, M Dewhirst, and M Oldham. A comprehensive method for optical-emission computed tomography. *Physics in Medicine and Biology*, 55(14):3947–3957, June 2010.

[45] M J Boot, C H Westerberg, J Sanz-Ezquerro, J Cotterell, R Schweitzer, M Torres, and J Sharpe. In vitro whole-organ imaging: 4D quantification of growing mouse limb buds. *Nature Methods*, 5(7):609–612, May 2008.

[46] C Vinegoni, C Pitsouli, D Razansky, N Perrimon, and V Ntziachristos. In vivo imaging of Drosophila melanogaster pupae with mesoscopic fluorescence tomography. *Nature Methods*, 5(1):45–47, December 2008.

[47] J F Colas and J Sharpe. Live optical projection tomography. *Organogenesis*, 5(4):211–216, 2009.

[48] M Oldham, H Sakhalkar, T Oliver, G Allan Johnson, and M Dewhirst. Optical clearing of unsectioned specimens for three-dimensional imaging via optical transmission and emission tomography. *Journal of Biomedical Optics*, 13(2):021113, 2008.

[49] H S Sakhalkar, M Dewhirst, T Oliver, Y Cao, and M Oldham. Functional imaging in bulk tissue specimens using optical emission tomography: fluorescence preservation during optical clearing. *Physics in Medicine and Biology*, 52(8):2035–2054, March 2007.

[50] D Hanahan and R A Weinberg. Hallmarks of Cancer: The Next Generation. *Cell*, 144(5):646–674, March 2011.

[51] A T Soufan, J M Ruijter, M J B van den Hoff, P A J de Boer, J Hagoort, and A F M Moorman. Three-dimensional reconstruction of gene expression patterns during cardiac development. *Physiological genomics*, 13(3):187–195, 2003.

[52] J McGinty, K B Tahir, R Laine, C B Talbot, C Dunsby, M A A Neil, L Quintana, J Swoger, J Sharpe, and P M W French. Fluorescence lifetime optical projection tomography. *Journal of Biophotonics*, 1(5):390–394, October 2008.

[53] J McGinty, H B Taylor, L Chen, L Bugeon, J R Lamb, M J Dallman, and P M W French. In vivo fluorescence lifetime optical projection tomography. *Biomedical optics express*, 2(5):1340–1350, 2011.

[54] A Bassi, D Brida, C D'Andrea, G Valentini, R Cubeddu, S De Silvestri, and G Cerullo. Time-gated optical projection tomography. *Optics letters*, 35(16):2732–2734, 2010.

[55] A Hörnblad, A Cheddad, and U Ahlgren. An improved protocol for optical projection tomography imaging reveals lobular heterogeneities in pancreatic islet and -cell mass distribution. *Islets*, 3(4):204–208, July 2011.

[56] R A Lorbeer, M Heidrich, C Lorbeer, D F Ramírez Ojeda, G Bicker, H Meyer, and A Heisterkamp. Highly efficient 3D fluorescence microscopy with a scanning laser optical tomograph. *Optics Express*, 19(6):5419–5430, 2011.